Coupled Modelling of ZrO_2/α-Zr(O) Layers Growth under Thermal and Mechanical Gradients

J-B. Minne[1,2], V. Optasanu[2,*] and T. Montesin[2]

[1]*CS, 22 av. Galilee, 92350 Le Plesis-Robinson, France*

[2]*ICB, UMR 6303 CNRS - Universit_e de Bourgogne Franche Comte 9, av. Alain Savary 21078 Dijon Cedex, France*

Abstract: The oxidation process of a nuclear reactor fuel rod clad made of zirconium is simulated. It is assumed that the oxygen is transported by anionic diffusion in the zirconia layer (ZrO2). Part of this oxygen reacts at the interface between the zirconia layer and the metal, while the rest diffuses in the oxygen-enriched metal volume (α-Zr(O)) to the core of the metal by an interstitial mechanism. The model is based on the thermodynamics of irreversible processes and takes into account the influence of driving forces on the oxygen migration in the metal such as the oxygen concentration gradient, the temperature gradient [1] and the mechanical stress gradient [2]. The growth of both ZrO2 and α-Zr(O) layers are simulated using the finite element software CAST3M. This model has been applied on an axisymmetric geometry by imposing a heat flow on the fuel side and a constant temperature on the waterside of the clad. The differences obtained in the inner and outer sides of the nuclear clad concerning the oxidation kinetics and oxygen distribution are related to some coupling parameters. Several values of those parameters are used in the simulations to highlight their influence on the oxidation behavior. Thus, we show that negative values for the heat of transport, which relates the gradient of ocncentration and the gradient of temperature, give coherent results with experimental observations on oxidation kinetics for both sides of the clad.

Keywords: Zirconium oxidation, thermal-mechanical-diffusion coupled modelling, non-equilibrium thermodynamics.

1. INTRODUCTION

Zirconium alloys used as clad material for fuel rods in water-cooled nuclear reactors, have given excellent service for many decades. Nevertheless, the corrosion of these alloys in high temperature water limits their service life and remains an interesting research issue nowadays. The zirconium oxidation reaction takes place at the metal/zirconia interface. It is based on the anionic diffusion of oxygen ions from the external environment to the metal/zirconia interface through the zirconia layer and via the interstitial diffusion of oxygen in the metal. The consequence of the diffusion through the oxide scale brings a diffusion-limited oxidation process and a cubic or parabolic oxidation rate, as long as the zirconia layer remains protective (the so-called pre-transition regime). After a thickness of a few micrometers, the zirconia layer exhibits a loss of its protective nature which leads to an acceleration of the oxidation rate (post-transition regime). The cyclic stages of cubic/parabolic kinetics, related to periodic destabilizations of the protective zirconia layer, constitute a general pattern for zirconium alloys at service temperatures and explain the linear kinetics which is often observed [3, 4]. It has been shown that, as the zirconia layer grows, mechanical stresses develop in the zirconia layer but also in the α-Zr(O) phase and could explain differences between experimental isothermal kinetics and analytical kinetics derived from the Wagner's theory [5].

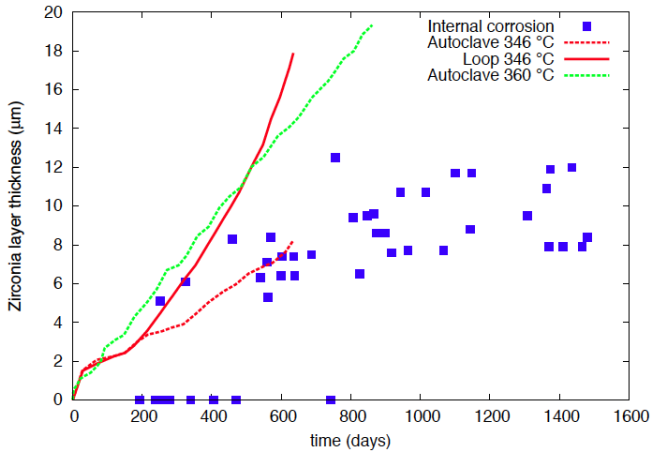

Figure 1: Out-of-pile experimental kinetics in autoclave at 346 [4] and 360 [3], in out-of-pile corrosion loop at 346 [4] and in-pile kinetics for innerside temperatures between 360 and 400 [6].

In reactor conditions, a heat flux is generated by the nuclear fuel contained in the Zr-alloy clad. As the zirconia layer grows, this heat flux increases the temperature at the metal/zirconia interface. However, waterside corrosion kinetics measured under constant heat flux in out-of-pile corrosion loops are greater than the kinetics measured under isothermal conditions in autoclaves (Figure **1**). It appears that the heat flux acts

Address correspondence to this article at the ICB, UMR 6303 CNRS - Universit_e de Bourgogne Franche Comte 9, av. Alain Savary 21078 Dijon Cedex, France; Tel: +33.380.39.91.84;
E-mail: virgil.optasanu@u-bourgogne.fr

E-ISSN: 2410-4701/19 © 2019 Zeal Press

as an additional driving force, through the temperature gradient, causing the acceleration of the corrosion kinetics [4]. On the inner side of the clad, a zirconia layer is generated by contact with the UO2 pellet. It grows very quickly up to 5 m, which is related to the implantation of fission products coming from the pellet over this thickness and then grows slowly up to a dozen micrometers and seems to progress no more [6] (Figure **1**). This zirconia layer seems to remain protective as it is stabilized in the tetragonal phase mostly by the fission products and because no acceleration of the kinetics is observed, contrary to waterside corrosion [2].

The purpose of this study is focused on the oxidation process on the outer and inner side of a nuclear fuel rod clad made of zirconium under thermal and mechanical gradients. We develop a coupled modelling of zirconium oxidation, including mechanical stresses and heat flux generated by the nuclear fuel. Such a coupling is classically achieved within the framework of irreversible thermodynamics.

2. THEORY OF DIFFUSION COUPLED TO HEAT AND MECHANICS

The classical theory of thermodynamics of irreversible processes provides an expression coupling the diffusion flux J of a particle in a solid and the heat flux q [1]:

$$J = -L_{11}\frac{\nabla_T \mu}{T} + L_{12}\nabla\frac{1}{T} \tag{1}$$

where μ is the chemical potential of the particle per unit of mass, T the temperature, ∇T the gradient of temperature and ∇_T the part of the gradient operator for which the temperature remains constant. L_{11} and L_{12} are phenomenological coefficients which relate the diffusion flux and the heat flux to the thermodynamics forces. $\nabla(1/T)$ is the force related to the heat flux and $-(\nabla_T \mu)/T$ is the force related to the diffusion flux. We consider here only the flux of one type of particle in the solid (e.g. oxygen in zirconium).

The heat of transport of the particle in the solid is introduced as followed:

$$Q = \frac{L_{12}}{L_{11}} \tag{2}$$

This quantity represents the heat transported per mole of particle in the absence of a temperature gradient.

Taking into account mechanical stress, the chemical potential is expressed as [5]:

$$\mu(c,T) = \mu^0(T) + RT\ln(c) - V_0\eta_{ij}\sigma_{ij} \tag{3}$$

in which μ^0 is the chemical potential of the particle in the reference state, c the mass fraction, V_0 the molar volume of the solid in the reference state and η_{ij} the chemical expansion coefficients. The concentration is defined according to the elemental volume of the solid in its reference state.

Assuming no temperature gradient and no mechanical stress, the diffusion flux in equation 1 is reduced to the Fick's law:

$$J = -\frac{L_{11}R}{c}\nabla c = -D\nabla c \tag{4}$$

in which D is the diffusion coefficient of the particle in the solid.

From equations 2 and 4, we can deduce the phenomenological coefficients:

$$L_{11} = \frac{Dc}{R} \; and \; L_{12} = \frac{DQc}{R} \tag{5}$$

For our calculations, the concentration is expressed in kg/m^3 and the diffusion flux in kg/(m$^{2.s}$). It is given, according to the previous equations, by:

$$J = -D\nabla c - \frac{DQc}{RT^2}\nabla T + \frac{M_0 Dc}{RT}\nabla\left(\eta_{ij}\sigma_{ij}\right) \tag{6}$$

where M_0 is the molar mass of the solid in the reference state.

The total reversible strain is classically expressed as the sum of the elastic strain, the thermal strain and the chemical strain:

$$\varepsilon_{ij}^{(r)} = \varepsilon_{ij}^{(e)} + \varepsilon_{ij}^{(th)} + \varepsilon_{ij}^{(ch)} \tag{7}$$

Thermal and chemical strains are expressed as followed:

$$\varepsilon_{ij}^{(th)} = \alpha_{ij}(T)\Delta T \; and \; \varepsilon_{ij}^{(ch)} = \eta_{ij}(c)\Delta c \tag{8}$$

where α_{ij} are the thermal expansion coefficients.

The mechanical stress tensor is given by the generalized Hook's law:

$$\sigma_{ij} = C_{ijkl}(c,T)\varepsilon_{kl}^{(e)} \tag{9}$$

where C_{ijkl} are the elastic components.

Evolutions of c, T and σ_{ij} with space and time are obtained by solving the equation of mass conservation,

$$\frac{\partial c}{\partial t} = -\nabla \cdot J \tag{10}$$

the heat equation,

$$\rho C_p \frac{\partial T}{\partial t} = -\nabla \cdot q \tag{11}$$

where q is given by Fourier's law:

$$q = -\lambda \nabla T \tag{12}$$

and the equation of local mechanical equilibrium.

$$\nabla \sigma = 0 \tag{13}$$

3. PHYSICAL DATA

Data used in our numerical simulations are presented in Table **1**. Elastic properties are expressed in the global coordinate system. They were calculated according to the properties measured in the crystallographic orientations of the α-Zr monocrystal [7] and related to the global system using the Kearns parameters [8], which enable to take into account the anisotropic properties and the texture of the metal. These Kearns parameters are given in normal, tangential and longitudinal directions: $f_n = 0.613$, $f_t = 0.328$ and $f_l = 0.074$. Thermal and chemical strains are also expressed in the global directions according to the thermal and chemical strains measured in the monocrystal orientations a and c: $\varepsilon_i = \varepsilon_c f_i + \varepsilon_a (1 - f_i)$ where i refers to the normal, tangential or longitudinal direction.

Table 1: Material properties used for the computations. c refers to the oxygen concentration in kg/m^3 and T refers to the temperature in Kelvin. Subscripts a and c refer to the directions a and c of the α-Zr monocrystal. The chemical strain in the ZrO_2 is not considered, as the diffusion occurs in grain boundaries

Properties	ZrO_2	α-Zr(O)
Elastic components in the global directions (GPa) [9, 7]	$C_{11} = 375$ $C_{21} = 156$ $C_{22} = 375$ $C_{31} = 94$ $C_{32} = 94$ $C_{33} = 219$ $C_{44} = 75$	$C_{11} = 167.9 + 0.165c - 0.041T$ $C_{21} = 64.0 + 0.061c - 0.008T$ $C_{22} = 162.3 + 0.153c - 0.043T$ $C_{31} = 65.5 + 0.023c + 0.011T$ $C_{32} = 67.0 - 0.013c + 0.014T$ $C_{33} = 157.6 + 0.135c - 0.044T$ $C_{44} = 40.9 + 0.099c - 0.024T$
Thermal strain [10, 11]	$\varepsilon^{th} = 7.8 \times 10^{-6} T - 2.34 \times 10^{-3}$	$\varepsilon_a^{th} = 5.1679 \times 10^{-6} T - 1.5603 \times 10^{-3}$ $\varepsilon_c^{th} = 4.5606 \times 10^{-6} T - 1.7734 \times 10^{-3}$
Chemical strain [12]	$\varepsilon_a^{ch} = 2.2251 \times 10^{-5} c + 5.0982 \times 10^{-8} c^2 - 1.8103 \times 10^{-10} c^3$ $\varepsilon_c^{ch} = 3.439 \times 10^{-5} c - 8.2121 \times 10^{-8} c^2 + 1.2237 \times 10^{-10} c^3$	
Zr → ZrO_2 transformation strain [9]	$\varepsilon_{\theta\theta} = \varepsilon_{zz} = 0.005$ $\varepsilon_{rr} = 0.54$	
Density (kg/m^3) [10]	$5800\left(1 - tr\left(\varepsilon^{th}\right)\right)$	$6550\left(1 - tr\left(\varepsilon^{th}\right) - tr\left(\varepsilon^{ch}\right)\right)$
Specific heat (J/kg/K) [10]	$565 + 6.11 \times 10^{-2} T - 1.14 \times 10^{7} T^{-2}$	0.1147T+252.55
Thermal conductivity (W/m/K) [10, 14]	$0.835 + 1.81 \times 10^{-4} T$	depends on T and c
Diffusion coefficient (cm^2/s) [13]	$1.05 \times 10^{-3} \exp\left(-\frac{122591}{RT}\right)$	$4.57 \times 10^{-4} \exp\left(-\frac{146440}{RT}\right)$

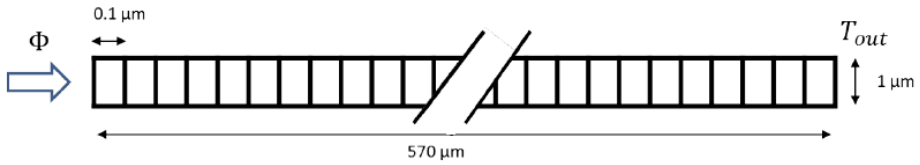

Figure 2: Geometry used for the simulations.

4. NUMERICAL RESOLUTION

The equations presented in section 2 are solved by the finite element method, using the software CASTEM 2014. Modifications have been introduced in the numerical convergence loop according to the equation 6. Mechanical stresses and temperature are calculated in steady state because they reach equilibrium much quicker than oxygen concentration. The clad is modelized by an axisymmetric mesh (Figure **2**). A constant heat flux is imposed on the inner face of the clad and a constant temperature ($T_{out} = 362°C$) on the outer face. A constant oxygen concentration is also imposed on these two faces. The two other faces of the geometry are imposed to remain parallel to the radial direction.

An isotropic thermal model is used to solve the thermal equations and an anisotropic elastic mechanical model to solve the mechanical equations. An isotropic thermal model with phase change is used to solve the diffusion equations, according to the analogy between thermal and diffusion equations. The value of the phase change temperature is set to the solubility concentration of oxygen in zirconium (464kg/m^3) and the latent heat is set to the concentration jump at the interface between the zirconia and the metal (1778kg/m^3). In order to avoid this concentration discontinuity in our calculations, we set the stoichiometric concentration of oxygen in zirconia as the difference between the actual concentration (2277kg/m^3) and the concentration jump. Hence, oxygen concentration is made continuous and the problem can be solved in one single domain of definition. The position of the interface between the zirconia and the metal is given by the value of oxygen concentration at the solubility concentration.

A previous study [5] showed that for such an axisymmetric configuration, the gradient of $\eta_{ij}\sigma_{ij}$ is very small in the zirconia layer and then, the mechanical effect on diffusion flux is insignificant. Moreover, the heat of transport of oxygen in zirconia is reported to be very small, if not zero [15]. However, in the α-Zr phase, its value is not known. In order to evaluate this parameter, we present numerical simulations of the growth of zirconia layers on the inner and the outer sides of a clad under heat flux using our model for the diffusion of oxygen in the α-Zr phase only. On the basis of corrosion experiments in autoclave and corrosion loops [3], we determine a value of the heat of transport and discuss the influence of temperature gradients on the waterside and innerside corrosion of the nuclear clad.

5. RESULTS AND DISCUSSION

Simulations of zirconia growth have been made for two different heat fluxes (60 and 100 W/cm^2). Six values of the heat of transport were investigated: $\pm 10^7$, $\pm 5 \times 10^7$ and $\pm 10^8 J/mol$. Calculations without thermal coupling (mechano-chemical coupling) and with no coupling at all (Fick's law) were also performed for comparison.

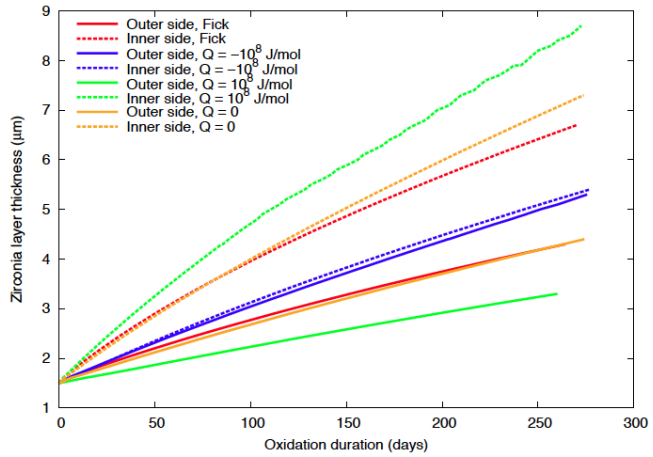

Figure 3: Simulated kinetics for $\Phi = 60W/cm^2$.

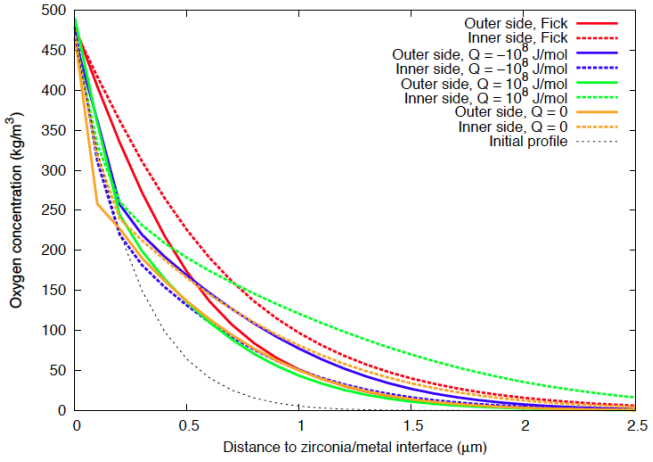

Figure 4: Radial distribution of the oxygen concentration in the metal for $\Phi = 60W/cm^2$ at the end of the simulation.

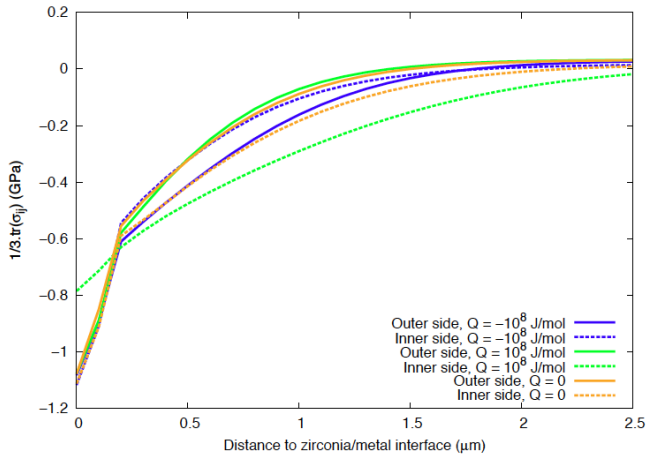

Figure 5: Radial distribution of the hydrostatic stress in the metal for $\Phi = 60W/cm^2$ at the end of the simulation.

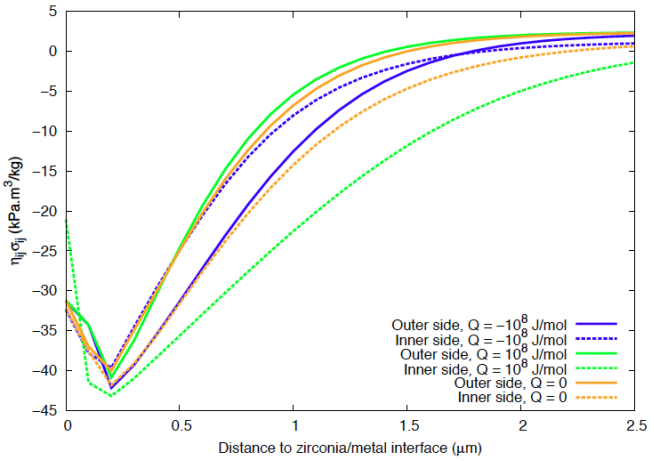

Figure 6: Radial distribution of the mechanical term $\eta_{ij}\sigma_{ij}$ in the metal for $\Phi = 60W/cm^2$ at the end of the simulation.

Some evolutions of the zirconia layer thickness with time are given in Figure **3** for $\Phi = 60W/cm^2$. The growth rate of the zirconia layer is higher on the inner side than on the outer side. This is coherent with a higher temperature on the inner side, because of the direction of the heat flux. However, each coupling moderate more or less this growth rate. Comparisons between the case without coupling (Fick) and the case without thermal coupling ($Q = 0$) show that there is little difference on the outer face while the zirconia layer grows faster on the inner side when considering the mechano-chemical coupling. When considering the full coupling, positive values of Q accelerate the zirconia growth on the inner side while they diminish it on the outer side. For negative values of Q, the trends are switched. This latter case corresponds qualitatively to the observations made on separate analytical experiments in thermal loops and in autoclave (Figure **1**). Considering the kinetics on the inner side of the clad, the heat flux has a slowing down effect on the oxidation, which is coherent with the experimental observations that the zirconia layer thickness remains bounded to a dozen micrometers.

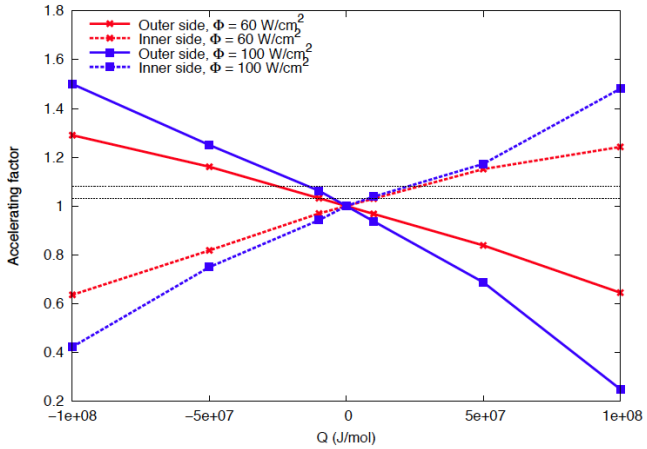

Figure 7: Accelerating factor versus heat of transport for $\Phi = 60W/cm$ (in red) and $\Phi = 100W/cm^2$ (in blue).

The corresponding oxygen concentration profiles in the metal are showed Figure **4**. While profiles for the case without coupling are morphologically similar to the initial profile, we can note a particular change around $c = 250kg/m^3$ for the other cases. This change of oxygen concentration gradient is related to the mechanical coupling and is coherent with previous calculations [5]. It is most particularly connected to the variation of the parameter a of the zirconium hexagonal lattice with the oxygen concentration. The diffusion depths of oxygen in the metal are directly related to the growth rates of the zirconia layer: the thicker the zirconia layer is, the deeper the oxygen diffuses.

For each coupled case, we determined an accelerating factor. It is defined as the ratio of zirconia layer thicknesses between the coupled case and the case without thermal coupling ($Q = 0$). Figure **7** represents the evolution of this factor with the heat of transport on the inner side and the outer side of the clad. As it is suggested by the kinetics, increasing the heat of transport increases this factor on the inner side but decreases it on the outer side. This factor was experimentally deduced for the same thermal boundary conditions used in our simulations: 1.03 at 60W/cm^2 and 1.08 at 100W/cm^2 [3]. From this two values, we can predict a value of the heat of transport around -2 x 10^{7}J/mol (Figure **7**).

Compared to known heats of transport of interstitial oxygen diffusing in metals of groups 4 and 5 (β-Zr, Ta,

Nb and V, cf. Table **2**), the proposed value turns out to be too high of 2 or 3 orders of magnitude. In the β-Zr phase, it was reported to be 89.1 kJ/mol between 1400 and 1700 [1]. These authors also suggest that this value should be negative in α-Zr according to experimental observations. The big value that our simulations suggest for the heat transfer in α-Zr tend to show that the thermally driven diffusion is probably not the only factor that can explain the difference between the nuclear clad inner and outer sides oxidation. However, for negative heat of transport values, the thermomigration acts in the same sense as the experimental observations. Thus, experimental investigations would be necessary to measure the heat of transport in α-Zr.

Table 2: Heat of transport of interstitial oxygen for some metals of groups 4 and 5

Metal	Q (kJ/mol)	Ref.
α-Zr	−20000	this work
β-Zr	89.1	[1]
Ta	−20 to −80	[16]
Nb	−67	[16]
V	17 to 29	[16]

6. CONCLUSIONS

By means of a thermodynamic approach, we developed a coupled modelling of zirconia layer growth under thermal and mechanical gradients, taking into account the oxygen diffusion in zirconium. The heat of transport of oxygen in α-Zr, which relates the thermal gradient to the oxygen diffusion flux, remains experimentally unevaluated, as for we know. We built a methodology in order to determine its value, based on experimental data of the open literature. It was shown that this parameter is necessary negative, which is coherent with an accelerating effect on the outer side and a slowing down effect on the inner side. The value of the heat of transport obtained by our simulations in order to fit the experimental observations is about 2 orders of magnitude bigger than values for other materials, which suggests that the thermomigration is probably not the only factor that can explain the differences experimentally observed between the oxidation of the inner and outer sides of the nuclear clad. However, experimental works should measure the α-Zr heat of transport in order to evaluate the importance of the thermotransport in strong temperature gradients oxidizing environments.

REFERENCES

[1] Vogel DL, Rieck GD. Thermotransport of nitrogen and oxygen in b-zirconium. Acta Metallurgica 1971; 19: 233-245. https://doi.org/10.1016/0001-6160(71)90151-9

[2] Minne J-B. Contribution à la modélisation du couplage mécanique/chimique de l'évolution de l'interface pastille-gaine sous irradiation, PhD Thesis, Université de Bourgogne 2013.

[3] Bouineau V, Ambard A, Bénier G, Pêcheur D, Godlewki J, Fayette L, Duverneix T. A new model to predict the oxidation kinetics of zirconium alloys in a pressurized water reactor. Journal of ASTM International 2008; 5(5): 1-23. https://doi.org/10.1520/JAI101312

[4] Billot P, Beslu P, Giordano A, Thomazet J. Development of a mechanistic model to assess the external corrosion of the Zircaloy claddings in PWRs, 8th International Symposium on Zirconium in the Nuclear Industry. ASTM STP 1989; 1023: 165-186. https://doi.org/10.1520/STP18864S

[5] Favergeon J, Montesin T, Bertrand G. Mechano-chemical aspects of high temperature oxidation: a mesoscopic model applied to zirconium alloys. Oxidation of Metals 2005; 64: 253-279. https://doi.org/10.1007/s11085-005-6563-7

[6] Desgranges L. Internal corrosion layer in PWR fuel, Seminar Proceedings on Thermal Performance of High Burn-Up LWR Fuel. OECD 1998; 187-196.

[7] Tremblay M, Roy C. Elastic parameters of single crystal Zr-O alloys. Materials Science and Engineering 1973; 12: 235-243. https://doi.org/10.1016/0025-5416(73)90034-7

[8] Nakatsuka M. Elastic anisotropy of zirconium alloy fuel cladding. Nuclear Engineering and Design 1981; 65: 103-112. https://doi.org/10.1016/0029-5493(81)90124-2

[9] Parise M, Sicardy O, Cailletaud G. Modelling of the mechanical behavior of the metal-oxide system during Zr alloy oxidation. Journal of Nuclear Materials 1998; 256: 35-46. https://doi.org/10.1016/S0022-3115(98)00045-2

[10] MATPRO - A Library of Materials Properties for Light-Water-Reactor Accident Analysis, NUREG/CR-6150, Vol. 4, Rev. 2 2001.

[11] Goldak J, Lloyd LT, Barrett CS. Lattice parameters, thermal expansions and Grüneisen coefficients of zirconium, 4.2 to 1130 K. Physical Review 1966; 144: 478-484. https://doi.org/10.1103/PhysRev.144.478

[12] Holmberg B, Dagerhamn T. X-ray studies on solid solutions of oxygen in alpha-zirconium. Acta Chemica Scandinavica 1961; 15: 919-925. https://doi.org/10.3891/acta.chem.scand.15-0919

[13] Debuigne J. Contribution à l'étude de l'oxydation du zirconium et de la diffusion de l'oxygène dans l'oxyde et dans le métal, PhD Thesis, Université de Paris 1966.

[14] Bunnell LR, Bates JL, Mellinger GB. Some high-temperature properties of Zircaloy-oxygen alloys. Journal of Nuclear Materials 1983; 116: 219-232. https://doi.org/10.1016/0022-3115(83)90106-X

[15] Ahlgren EO, Poulsen FW. Thermoelectric power of stabilized zirconia. Solid State Ionics 1995; 82: 193-201. https://doi.org/10.1016/0167-2738(95)00201-3

[16] Mathuni J, Kirchheim R, Fromm E. Thermotransport of oxygen in tantalum base alloys. Acta Metallurgica 1979; 27: 1665-1669. https://doi.org/10.1016/0001-6160(79)90048-8

Received on 05-09-2019 Accepted on 20-09-2019 Published on 25-09-2019

DOI: https://doi.org/10.31875/2410-4701.2019.06.2

© 2019 Minne *et al*.; Zeal Press
This is an open access article licensed under the terms of the Creative Commons Attribution Non-Commercial License (http://creativecommons.org/licenses/by-nc/3.0/) which permits unrestricted, non-commercial use, distribution and reproduction in any medium, provided the work is properly cited.